Ultrabroadband reflective polarization convertor for terahertz waves

Yong Zhi Cheng,[1,2] Withawat Withayachumnankul,[1,3,a)] Aditi Upadhyay,[3] Daniel Headland,[1] Yan Nie,[2] Rong Zhou Gong,[2] Madhu Bhaskaran,[3] Sharath Sriram,[3,b)] and Derek Abbott[1]
[1]*School of Electrical and Electronic Engineering, The University of Adelaide, Adelaide, South Australia 5005, Australia*
[2]*School of Optical and Electronic Information, Huazhong University of Science and Technology, Wuhan 430074, China*
[3]*Functional Materials and Microsystems Research Group, School of Electrical and Computer Engineering, RMIT University, Melbourne, Victoria 3001, Australia*

(Received 29 August 2014; accepted 28 October 2014; published online 6 November 2014)

We design and experimentally demonstrate an ultrathin, ultrabroadband, and highly efficient reflective linear polarization convertor or half-wave retarder operating at terahertz frequencies. The metamaterial-inspired convertor is composed of metallic disks and split-ring resonators placed over a ground plane. The structure exhibits three neighboring resonances, by which the linear polarization of incident waves can be converted to its orthogonal counterpart upon reflection. For an optimal design, a measured polarization conversion ratio for normal incidence is greater than 80% in the range of 0.65–1.45 THz, equivalent to 76% relative bandwidth. The mechanism for polarization conversion is explained via decomposed electric field components that couple with different resonance modes of the structure. The proposed metamaterial design for enhancing efficiency of polarization conversion has potential applications in the area of terahertz spectroscopy, imaging, and communications. © *2014 AIP Publishing LLC*. [http://dx.doi.org/10.1063/1.4901272]

Terahertz science and technology have seen rapid development, underpinned by many promising applications in imaging, sensing, and communications.[1] Towards these applications, high-performance terahertz components become essential for manipulating terahertz waves. One important group of components is related to polarization manipulation, including polarizers, wave retarders, and polarization rotators. In particular, conventional wave retarders can be achieved by using waveplates made of natural birefringent materials with a retardation effect.[2,3] Those wave plates require a relatively long propagation distance to obtain sufficient phase accumulation, despite the limited operation bandwidth and availability. Thus, more convenient and flexible approaches are desirable to fully manipulate the polarization state of electromagnetic waves.

Over the past decade, metamaterials as artificial composite materials have attracted great attention due to their exotic electromagnetic properties unavailable to natural materials.[4] Such unique properties open up significant opportunities, including an alternative approach to manipulating the polarization of electromagnetic waves.[5–9] Several high-efficiency wave retarders have been demonstrated through different metamaterial microstructure designs, and these polarization wave retarders were demonstrated for conversion between different polarization states, such as linear to linear,[10–14] linear to circular,[15,16] and circular to circular polarization.[17] Compared with the traditional wave plates, these metamaterial-based wave retarders have advantages including subwavelength thickness, high conversion efficiency, angular tolerance, and scalability. In most of the existing wave retarders, the polarization states are manipulated in the transmission mode with a limited number of designs operating in the reflection mode.[11,12,15,18] For most retarders in the reflection mode, the undesirable high co-polarization reflection severely limits the polarization conversion efficiency and the bandwidth. To extend the functionality, broadband reflective polarization converters or retarders with high performance are highly desirable.

Here, we present design, fabrication, and characterization of an ultrathin and highly efficient half-wave retarder operating in the reflection mode at terahertz frequencies. Based on the concept of metamaterials, the retarder comprises an array of split-ring resonators (SRRs) and disk resonators (together henceforth referred to as DSRRs), which in conjunction can rotate the linear polarization by 90° with an extended operation bandwidth. An underlying physical mechanism of the observed polarization conversion is investigated through decomposed electric field components that interact with the DSRRs.

A schematic of the proposed reflective linear polarization convertor is shown in Fig. 1. A unit cell of the DSRR is composed of a metallic disk and split-ring resonator placed near to the ground plane and separated by a 30-μm thick

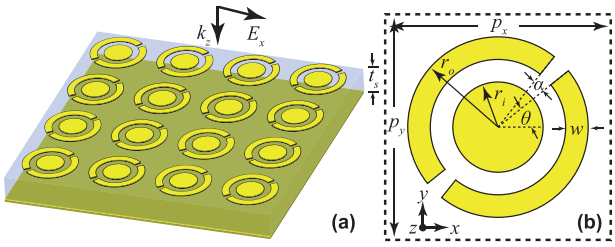

FIG. 1. Schematic of the proposed polarization converter: (a) A DSRR array and (b) a unit cell structure. The dimensions are as follows: $p_x = p_y = 110\ \mu$m, $t_s = 30\ \mu$m, $r_i = 28\ \mu$m, $r_o = 48\ \mu$m, $w = 12\ \mu$m, $\alpha = 6.8°$, and $\theta = 41.6°$.

a)Electronic mail: withawat@eleceng.adelaide.edu.au
b)Electronic mail: sharath.sriram@gmail.com

polydimethylsiloxane (PDMS) dielectric spacer. Specifically, the top metallic layer and the ground plane are made of 200 nm thick gold and platinum layers, respectively, to provide etch selectivity during microfabrication. The structure is periodic along the x and y axes with periods p_x and p_y of 110 μm to avoid diffraction at the normal incidence for frequencies up to 2.7 THz. As shown in Fig. 1(a), the DSRR orientation is such that incident waves with the polarization along the x or y axis is rotated by 90° to their orthogonal polarization state after reflecting off the structure.

The DSRR design shown in Fig. 1(a) has been fabricated with photolithography and metallization process steps. A ground plane made of a 200 nm platinum layer with a 20 nm thick titanium adhesion layer is deposited on a standard silicon substrate. The PDMS is subsequently prepared in a 1:10 ratio of curing agent to pre-polymer and spin-coated onto the platinum surface and cured. A spin speed of 1900 rpm with acceleration of 1000 rpm/s^2 and spin duration of 30 s are used. Then, a 200 nm gold layer with a 20 nm chromium adhesion layer is deposited. This metal bilayer is patterned to define the DSRR structure by photolithography and wet etching. The sample is then cleaned with solvents to strip residual photoresist in preparation for terahertz measurements. The sample measures $50 \times 50\,\text{mm}^2$ and is made up of 207,025 identical DSRRs with periodic arrangement. Figure 2 shows the microscopic images that reveal the details of a small area and a unit cell of the sample. Subsequent characterization of the sample with a surface/stylus profilometer shows that the actual PDMS thickness, t_s, is 45 μm, as opposed to the target of 30 μm.

The measurement utilizes a fiber-coupled terahertz time-domain spectrometer (THz-TDS), Tera K15 manufactured by Menlo Systems GmbH. For normal incidence, as shown in Fig. 3(a), a linearly polarized terahertz beam from an emitting photoconductive antenna (PCA) is collimated with a dielectric lens, directed through a linear polarizer and a beamsplitter, and then reflected normally from the sample. The reflected beam is then directed by the beamsplitter through a second polarizer into a second lens that focuses the energy onto the receiving PCA. Here, an ordinary 2-in. undoped float-zone silicon wafer with a thickness of 3.5 mm and resistivity of 10 kΩ·cm is used as a beamsplitter. A gold-coated mirror replaces the sample for reference measurement. For the 45° specular measurement, as shown in Fig. 3(b), the emitter and receiver antennas are each inclined in the x-z plane to an angle of ±45° with respect to the normal of the sample surface.

We define $r_{xx} = |\mathbf{E}_x^r|/|\mathbf{E}_x^i|$, $r_{yx} = |\mathbf{E}_y^r|/|\mathbf{E}_x^i|$, $r_{xy} = |\mathbf{E}_x^r|/|\mathbf{E}_y^i|$, and $r_{yy} = |\mathbf{E}_y^r|/|\mathbf{E}_y^i|$ as the reflection coefficients for different

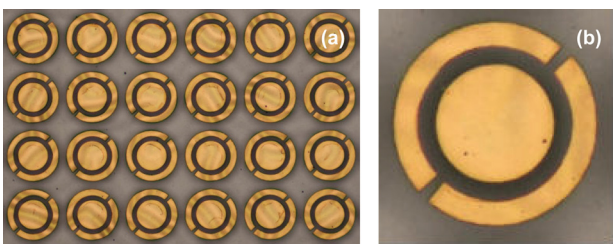

FIG. 2. Fabricated structure. Microscopic images for a small area (a) and a unit cell (b) of the convertor with dimensions in agreement with Fig. 1(b).

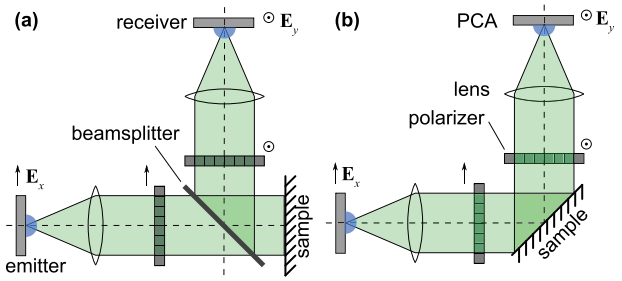

FIG. 3. Configurations of the fiber-coupled terahertz system for cross-polarization measurement. (a) Normal incidence and (b) oblique incidence at 45°.

polarization conversion. The superscripts i and r denote the incident and reflected terahertz waves, respectively, and the subscripts x and y indicate the polarization directions of terahertz waves, corresponding to the TM and TE polarizations, respectively. Due to the mirror symmetry along the diagonal axis of each DSRR, for the normal incidence, we need to consider only the incident x-polarized waves and determine the reflection coefficients r_{xx} and r_{yx}. During the measurement, we keep the transmitter x-polarized and measure the response with the receiver in either polarization by rotating the receiving PCA and the second polarizer about the optical axis. For all measurements, the total scanning duration time is 78 ps and is digitized with a step size of 0.078 ps.

In order to gain insight into the mechanism of the polarization conversion, simulations based on the finite element method (FEM) are performed by using the frequency-domain solver in CST Microwave Studio for the unit-cell structure. In the simulation, the relative permittivity and loss tangent of PDMS are 2.35 and 0.06, respectively, as determined from independent measurement.[19] The material parameters of the gold and platinum layers are explained by the surface impedance model with Drude parameters.[19] The PDMS thickness and DSRR geometrical parameters are given in Fig. 1.

Figures 4(a) and 4(b) show the magnitude of the reflection coefficients at normal incidence for the optimal and fabricated structures with the PDMS thicknesses t_s of 30 and 45 μm, respectively. It can be seen that the adjusted numerical results are in reasonable agreement with the measured results, and the discrepancies are likely caused by tolerances in fabrication and measurement. From the simulated reflection coefficients of the optimal structure in Fig. 4(a), three resonances: $f_1 = 0.71$ THz, $f_2 = 0.99$ THz, and $f_3 = 1.37$ THz, can be observed with the magnitude of the co-polarization reflection coefficient, r_{xx}, reaching the local minima of about 0.10, 0.05, and 0.10, respectively. These three resonance positions correspond to the high magnitude of the cross-polarization reflection coefficient r_{yx}. In Fig. 4(b), only two resonances can be observed in the fabricated sample, and the co-polarization component r_{xx} is high around 1.0 THz. For the optimal design, the measured magnitude of the cross-polarization component is greater than 50% from 0.58 to 1.52 THz, while the co-polarized component is less than 30% on average.

The polarization conversion ratio (PCR) is defined as $\text{PCR} = |r_{yx}|^2/(|r_{yx}|^2 + |r_{xx}|^2)$ for x-polarization incidence waves.[15] Figures 4(c) and 4(d) show the simulated and measured PCRs as a function of frequency. It is shown that the

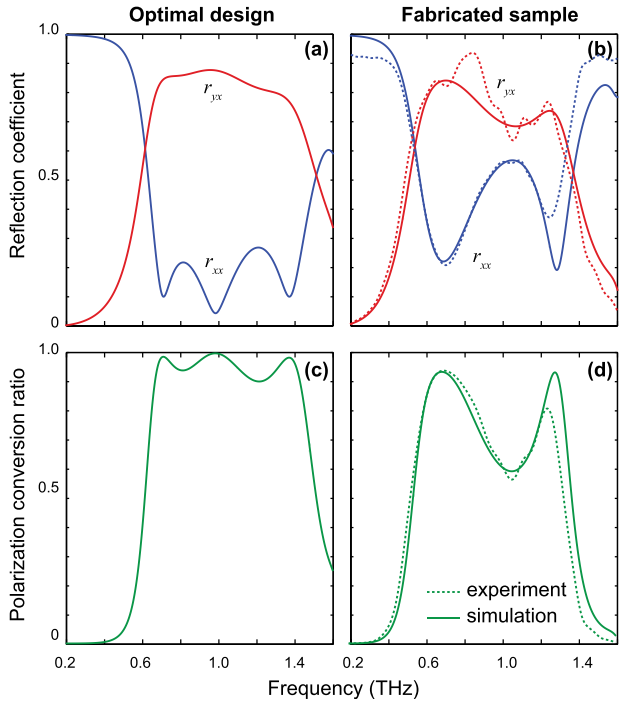

FIG. 4. Responses of the converter at normal incidence. Magnitude of the reflection coefficients r_{xx} and r_{yx} for the optimal design (a) and fabricated design (b). PCR for the optimal design (c) and fabricated design (d).

PCR of the optimal structure in Fig. 4(c) is roughly above 80% from 0.65 to 1.45 THz. Hence, the bandwidth relative to the center frequency is 76%. This achieved bandwidth is nearly twice as broad as that obtained from L-shaped antennas in the infrared regime.[12] For this optimal design, the PCR is greater than 95% at the three resonance frequencies, where nearly perfect polarization conversion takes place.

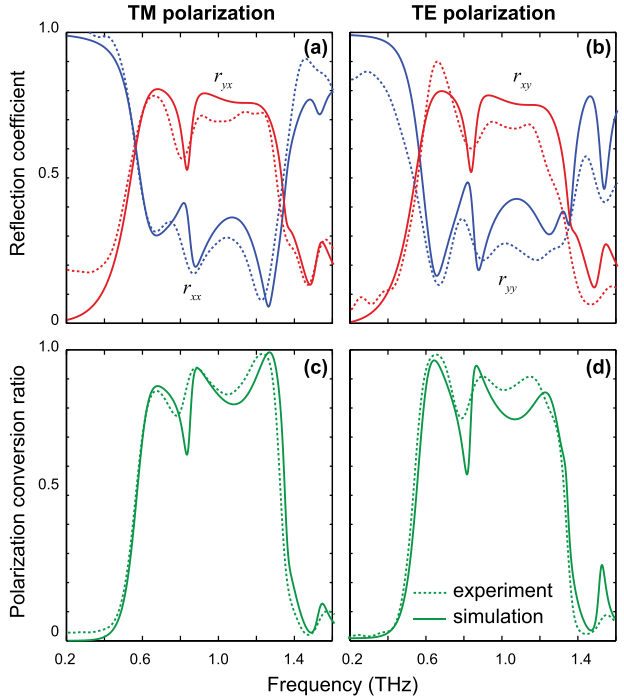

FIG. 5. Responses of the non-optimal converter at 45° oblique incidence. (a) and (b) The reflection coefficients for the TM and TE polarizations, respectively. (c) and (d) The PCRs for the TM and TE polarizations, respectively.

The broadband operation mainly originates from the superposition of multiple resonance modes. As for the fabricated non-optimal structure in Fig. 4(d), the PCR is degraded but can still be maintained over 50% from 0.53 to 1.36 THz. This reasonable performance demonstrates the robustness of the design to fabrication tolerances, particularly where the PDMS thickness is deviated by up to 150%.

Figure 5 shows the magnitude of the reflection coefficients of the non-optimal structure at 45° oblique incidence in the x-z plane with the TM and TE polarizations. The experimental and numerical results are in good agreement in general. For both of the polarizations, the measured magnitude of the cross-polarization reflection coefficients (r_{yx} and r_{xy}) is greater than 50% from 0.52 to 1.3 THz, while the co-polarization reflection coefficients (r_{xx} and r_{yy}) are less than 50%. The corresponding PCRs are greater than 75% at most points in this band as shown in Figs. 5(c) and 5(d). Those sharp spectral features are not resolved in the experiment because of the limited spectral resolution. It is clear that the bandwidth of the convertor can be reasonably sustained at a wide range of incidence angles.

The mechanism of the polarization convertor can be understood from resolved current distributions in relation to decomposed incident electric fields along the u and v axes, as shown in Fig. 6(d). At the lowest resonance frequency of 0.71 THz, each arc that constitutes the SRR behaves as a dipole resonator that couples with the $\mathbf{E}_v$ component, as shown in Fig. 6(a) and imparts a zero phase shift in reflection. At this frequency, the structure does not resonate with the $\mathbf{E}_u$ component, and hence a $-\pi$ phase shift is imparted on this component by the ground plane. At the second resonance, as shown in Fig. 6(b), the $\mathbf{E}_u$ component excites a set of shorter dipoles, which induces a 0° phase shift similarly to the first case. Since the $\mathbf{E}_v$ component is in this case reflected off by the ground plane, the phase difference between the two orthogonal components is equal to π. At the highest resonance, as shown in Fig. 6(c), both the disk and SRR are coupled with the $\mathbf{E}_v$ component, which is reflected off with a zero phase change, whilst the ground plane imparts the $\mathbf{E}_u$

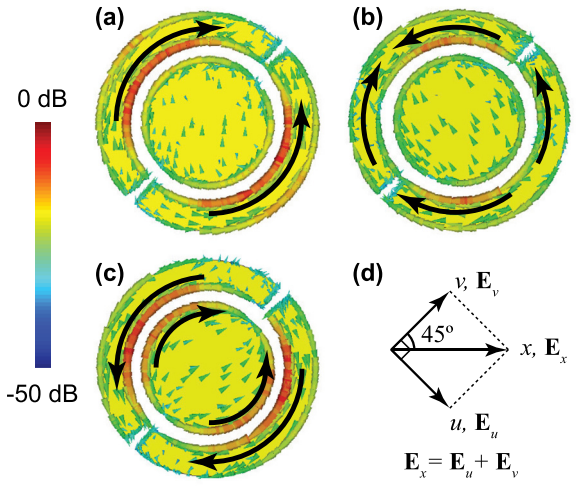

FIG. 6. Surface current distributions on the DSRR for incident x-polarized waves at the three resonances. (a) 0.71 THz, (b) 0.99 THz, and (c) 1.37 THz. All the plots are normalized to their respective maximum value and in logarithmic scale. (d) Schematic of the decomposed electric fields.

component with a $-\pi$ phase change. Therefore, at these resonance frequencies, the absolute phase difference between the reflected $\mathbf{E}_u$ and $\mathbf{E}_v$ components is always equal to π, which causes polarization rotation by 90° for the incident $\mathbf{E}_x$. This underlying mechanism for the phase difference is confirmed through the simulation with $\mathbf{E}_u$ and $\mathbf{E}_v$ excitations on the structure (not shown).

In conclusion, we have numerically and experimentally demonstrated an array of the DSRRs that functions as a broadband half-wave plate to convert the linear polarization of terahertz waves into its orthogonal polarization. The reflection-mode operation at terahertz frequencies offers an alternative to existing converters operating in transmission. For the optimal design, the polarization conversion ratio is greater than 80% in the frequency range between 0.65 and 1.45 THz, equivalent to 76% bandwidth. This high polarization conversion efficiency is ascribed to the three resonances that can be tuned via the DSRR geometry. Furthermore, the results show that this converter can tolerate the oblique incidence with an angle at least 45° for both the TE and TM polarizations. The proposed design can also be used to invert the handedness of the elliptically or circularly polarized waves and can be scaled to operation at other frequency ranges.

W.W. and D.A. acknowledge the Australian Research Council (ARC) Discovery Project DP120100200. M.B. and S.S. acknowledge ARC Postdoctoral Fellowships DP1092717 and DP110100262, respectively. S.S. acknowledges partial support from Victoria and AFAS-Vic Fellowships. Y.Z.C. and Y.N. acknowledge the National Natural Science Foundation of China (No. 51207060) and the foundation for Chinese Scholarship Council (No. 201306160039). Technical support from staff at the RMIT Microscopy and Microanalysis Facility is acknowledged, along with funding from the National Collaborative Research Infrastructure Scheme.

[1]B. Ferguson and X.-C. Zhang, Nat. Mater. **1**, 26 (2002).
[2]C.-Y. Chen, T.-R. Tsai, C.-L. Pan, and R.-P. Pan, Appl. Phys. Lett. **83**, 4497 (2003).
[3]J.-B. Masson and G. Gallot, Opt. Lett. **31**, 265 (2006).
[4]W. Withayachumnankul and D. Abbott, IEEE Photonics J. **1**, 99 (2009).
[5]T. Niu, W. Withayachumnankul, A. Upadhyay, P. Gutruf, D. Abbott, M. Bhaskaran, S. Sriram, and C. Fumeaux, Opt. Express **22**, 16148 (2014).
[6]J. Y. Chin, M. Lu, and T. J. Cui, Appl. Phys. Lett. **93**, 251903 (2008).
[7]N. K. Grady, J. E. Heyes, D. R. Chowdhury, Y. Zeng, M. T. Reiten, A. K. Azad, A. J. Taylor, D. A. Dalvit, and H.-T. Chen, Science **340**, 1304 (2013).
[8]Y. Cheng, Y. Nie, X. Wang, and R. Gong, Appl. Phys. A **111**, 209 (2013).
[9]H. Shi, A. Zhang, S. Zheng, J. Li, and Y. Jiang, Appl. Phys. Lett. **104**, 034102 (2014).
[10]L. Cong, W. Cao, X. Zhang, Z. Tian, J. Gu, R. Singh, J. Han, and W. Zhang, Appl. Phys. Lett. **103**, 171107 (2013).
[11]H. Cheng, S. Chen, P. Yu, J. Li, B. Xie, Z. Li, and J. Tian, Appl. Phys. Lett. **103**, 223102 (2013).
[12]Q. Lévesque, M. Makhsiyan, P. Bouchon, F. Pardo, J. Jaeck, N. Bardou, C. Dupuis, R. Haïdar, and J.-L. Pelouard, Appl. Phys. Lett. **104**, 111105 (2014).
[13]H. F. Ma, G. Z. Wang, G. S. Kong, and T. J. Cui, Opt. Mater. Express **4**, 1717 (2014).
[14]S.-C. Jiang, X. Xiong, P. Sarriugarte, S.-W. Jiang, X.-B. Yin, Y. Wang, R.-W. Peng, D. Wu, R. Hillenbrand, X. Zhang *et al.*, Phys. Rev. B **88**, 161104 (2013).
[15]J. Hao, Y. Yuan, L. Ran, T. Jiang, J. A. Kong, C. Chan, and L. Zhou, Phys. Rev. Lett. **99**, 063908 (2007).
[16]W. Sun, Q. He, J. Hao, and L. Zhou, Opt. Lett. **36**, 927 (2011).
[17]L. Wu, Z. Yang, Y. Cheng, R. Gong, M. Zhao, Y. Zheng, J. Duan, and X. Yuan, Appl. Phys. **116**, 643 (2014).
[18]M. Feng, J. Wang, H. Ma, W. Mo, H. Ye, and S. Qu, J. Appl. Phys. **114**, 074508 (2013).
[19]T. Niu, W. Withayachumnankul, B. S.-Y. Ung, H. Menekse, M. Bhaskaran, S. Sriram, and C. Fumeaux, Opt. Express **21**, 2875 (2013).